Supporting Information

For

Synchronously tuning the spin-crossover and fluorescent properties of a two-dimensional Fe(II) coordination polymer by solvent guests

Chun-Feng Wang*, Jin-Chuan Wu, Qing-Xin Li*

Guangdong Provincial Engineering Laboratory of Biomass High Value Utilization, Institute of Biological and Medical Engineering, Guangdong Academy of Sciences, Guangzhou, China.

E-mail: qingxin_li@outlook.com, cfwang@yzu.edu.cn

Table of Contents

Table S1. Crystal data and structure refinements for **1** at 100 and 300 K.

T / K	100 K	300 K
Empirical formula	$C_{56}H_{40}Fe_2N_{16}Pt_2$	$C_{56}H_{40}Fe_2N_{16}Pt_2$
Molecular weight	1438.92	1438.92
Crystal system	Triclinic	monoclinic
Space group	*P*-1	*I*2/*m*
a/Å	7.1309 (6)	22.121 (4)
b/Å	14.4549 (18)	7.4720 (7)
c/Å	21.5843 (11)	29.898 (7)
α/°	104.371 (7)	90
β/°	90.005 (6)	108.25 (2)
γ/°	92.605 (9)	90
Volume/Å^3	2152.8 (3)	4693.1 (16)
Z	1	2
ρ_{calc}g/cm^3	1.665	1.522
μ/mm^{-1}	13.282	12.078
F(000)	1044.0	2082.0
Crystal size/mm^3	0.10 × 0.08 × 0.04	0.10 × 0.08 × 0.04
Radiation	CuKα (λ = 1.54184)	CuKα (λ = 1.54184)
2Θ range for data collection/°	8.434 to 130.17	8.418 to 122.318
Reflections collected	12955	7720
unique	R_{int} = 0.0878	R_{int} = 0.1189
Goodness-of-fit on F^2	0.823	0.950
Final R indexes [I>=2σ (I)]	R_1 = 0.1081, wR_2 = 0.2714	R_1 = 0.0970, wR_2 = 0.2278
Final R indexes [all data]	R_1 = 0.2216，wR_2 = 0.3445	R_1 = 0.1370, wR_2 = 0.2547
Largest diff. peak/hole / e Å^{-3}	4.11/-4.87	3.81/-2.10

Table S2. Comparative analyses of selected bond lengths [Å] of **1** at 100 and 300 K.

T / K	Experimental data	
	100 K	300 K
Fe-NC	1.930(5)	2.150(12)
Fe-ppma	2.000(4)	2.180(14)

Table S3. Crystal data and structure refinements for **1·*x*H$_2$O** at 100, 145, 180 and 280 K.

T / K	100 K	145 K	180 K	280 K
Spin State, HS_nLS_{1-n}	$HS_{0.0}LS_{1.0}$	$HS_{0.5}LS_{0.5}$	$HS_{0.67}LS_{0.33}$	$HS_{1.0}LS_{0.0}$
Empirical formula	$C_{28}H_{20}Fe_1N_8Pt_1$	$C_{28}H_{20}Fe_1N_8Pt_1$	$C_{84}H_{60}Fe_3N_{24}Pt_3$	$C_{28}H_{20}Fe_1N_8Pt_1$
Molecular weight	719.62	719.62	2158.86	719.62
Crystal system	monoclinic	monoclinic	monoclinic	monoclinic
Space group	*C*2/*m*	*C*2/*m*	*C*2/*m*	*C*2/*m*
a/Å	28.064 (4)	28.079 (4)	29.4282 (10)	28.444 (2)
b/Å	7.1449 (6)	7.1349 (8)	7.3383 (2)	7.4354 (4)
c/Å	7.1665 (6)	7.1793 (5)	21.9432 (6)	7.3889 (3)
α/°	90	90	90	90
β/°	92.173 (10)	92.042 (9)	106.049 (3)	94.003 (5)
γ/°	90	90	90	90
Volume/Å^3	1435.9 (3)	1437.4 (3)	4554.0 (3)	1558.88(16)
Z	1	1	2	1
ρ_{calc}g/cm^3	1.664	1.662	1.574	1.533
μ/mm^{-1}	13.276	13.264	12.558	12.229
F(000)	696.0	696.0	2208.0	696.0
Crystal size/mm^3	0.10 × 0.08 × 0.04	0.10 × 0.08 × 0.04	0.10 × 0.08 × 0.04	0.10 × 0.08 × 0.04
Radiation	CuKα (λ = 1.54184)	CuKα (λ = 1.54178)	CuKα (λ = 1.54178)	CuKα (λ = 1.54178)
2Θ range for data collection/°	12.36 to 129.994	12.336 to 132.664	8.386 to 131.768	12.008 to 132.08
Reflections collected	5273	6181	37408	6811
unique	R_{int} = 0.0683	R_{int} = 0.0728	R_{int} = 0.0904	R_{int} = 0.0526
Goodness-of-fit on F^2	1.054	1.080	1.056	1.162
Final R indexes [I>=2σ (I)]	R_1 = 0.0720, wR_2 = 0.1762	R_1 = 0.0677, wR_2 = 0.1795	R_1 = 0.0627, wR_2 = 0.1652	R_1 = 0.0653, wR_2 = 0.1726
Final R indexes [all data]	R_1 = 0.0801，wR_2= 0.1881	R_1 = 0.0717, wR_2 = 0.1841	R_1 = 0.0685, wR_2 = 0.1719	R_1 = 0.0679, wR_2 = 0.1761
Largest diff. peak/hole / e Å^{-3}	4.58/-3.02	2.45/-1.80	5.64/-2.29	2.87/-1.02

Table S4. Comparative analyses of selected bond lengths [Å] of **1·*x*H$_2$O** at 100, 145 and 280 K.

T / K	Experimental data				
	100 K	145 K	180 K		280 K
	Fe1	Fe1	Fe1	Fe2	Fe1
Fe-NC	1.918 (8)	1.933 (7)	1.928 (7)	2.135 (7)	2.132 (9)
Fe-ppma	2.011 (2)	2.040 (14)	2.008 (6)	2.232 (10)	2.250 (10)

Table S5. Crystal data and structure refinements for **1**·***x*Solv** at 90, 160 and 250 K.

T / K	90 K	160 K	250 K
Empirical formula	$C_{57}H_{46}Fe_2N_{16}O_2Pt_2$	$C_{28}H_{20}Fe_1N_8Pt_1$	$C_{28}H_{20}Fe_1N_8Pt_1$
Molecular weight	1488.92	719.46	719.46
Crystal system	monoclinic	monoclinic	monoclinic
Space group	*I*2/*m*	*C*2/*m*	*C*2/*m*
a/Å	21.5106 (16)	28.246 (15)	28.471 (4)
b/Å	7.1465 (5)	7.3283 (17)	7.4361 (6)
c/Å	29.221 (2)	7.2809 (16)	7.3959 (6)
α/°	90	90	90
β/°	106.268 (8)	91.80 (3)	93.272 (9)
γ/°	90	90	90
Volume/Å^3	4312.1 (6)	1506.4 (9)	1563.2 (3)
Z	2	2	2
ρ_{calc}g/cm^3	1.701	1.586	1.528
μ/mm^{-1}	13.295	12.655	12.194
F(000)	2144.0	696.0	696.0
Crystal size/mm^3	0.10 × 0.08 × 0.04	0.10 × 0.08 × 0.04	0.10 × 0.08 × 0.04
Radiation	CuKα (*λ* = 1.54184)	CuKα (*λ* = 1.54184)	CuKα (*λ* = 1.54184)
2Θ range for data collection/°	8.564 to 119.962	12.162 to 122.212	11.986 to 119.89
Reflections collected	7045	2337	2451
unique	R_{int} = 0.0709	R_{int} = 0.0605	R_{int} = 0.0663
Goodness-of-fit on F^2	1.173	1.107	1.209
Final R indexes [I>=2σ (I)]	R_1 = 0.1106, wR_2 = 0.3077	R_1 = 0.1001, wR_2 = 0.2593	R_1 = 0.1050, wR_2 = 0.2704
Final R indexes [all data]	R_1 = 0.1264， wR_2 = 0.3243	R_1 = 0.1089, wR_2 = 0.2720	R_1 = 0.1131, wR_2 = 0.2814
Largest diff. peak/hole / e Å^{-3}	8.42/-4.32	3.61/-1.29	3.98/-2.43

Table S6. Comparative analyses of selected bond lengths [Å] of **1**·***x*Solv** at 90, 160 and 250 K.

T / K	Experimental data		
	90 K	160 K	250 K
Fe-NC	1.953(5)	2.020(14)	2.133(8)
Fe-ppma	2.006(3)	2.140(3)	2.230(6)

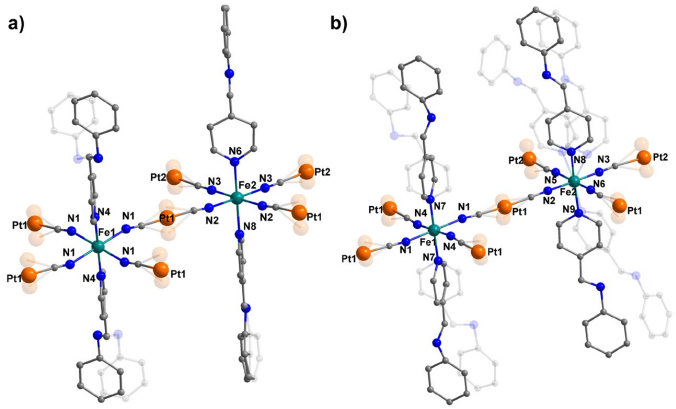

Fig. S1 Asymmetric units of compound **1** representative of (a) the parent cell (300 K) and (b) the phase-transition cell (100 K).

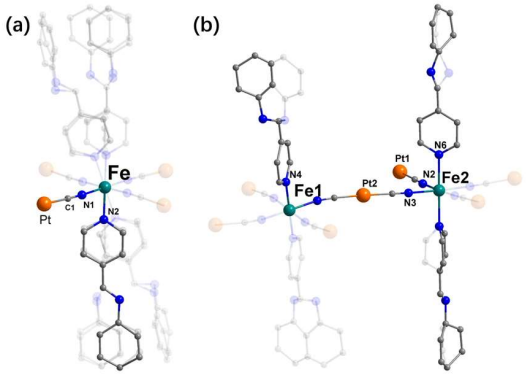

Fig. S2 Asymmetric unit of compound **1**·x**H₂O** at (**a**) 100 K and (**b**) 180 K. The asymmetric unit of compound **1**·x**H₂O**, which is constituted with 1/4 Fe(II) ion at 280, 145, and 100 K, contains two unique Fe(II) ions with occupies of 1/4 (Fe1) and 1/2 (Fe2), respectively, at 180 K.

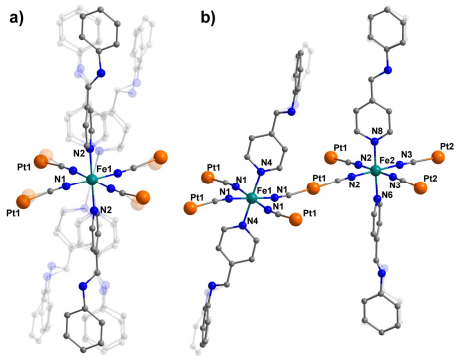

Fig. S3 Asymmetric units of compound **1·*x*Solv** representative of (a) the parent cell (250 K and 160 K) and (b) the phase-transition cell (90 K) showing structural transformation from $[Fe(ppma)_2Pt(CN)_4]$ to $[Fe_2^{II}(ppma)_4\{Pt(CN)_4\}_2]$.

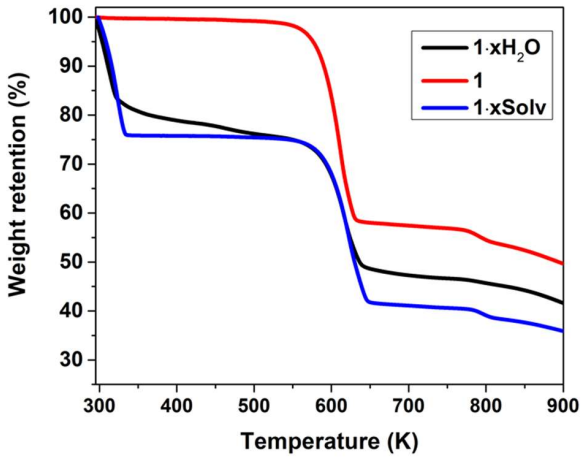

Fig. S4 TG analysis of **1·*x*H₂O**, **1**, and **1·*x*Solv**. The weight loss of *ca.* 21% in **1·*x*H₂O** and *ca.* 24% in **1·*x*Solv** are highly consistent with calculated results deduced from the elemental analyses of respective compounds, i.e., *ca.* 10 water molecules were included in the sample of **1·*x*H₂O**, and *ca.* 8 water molecules and 2 methanol molecules were included in the sample of **1·*x*Solv**.

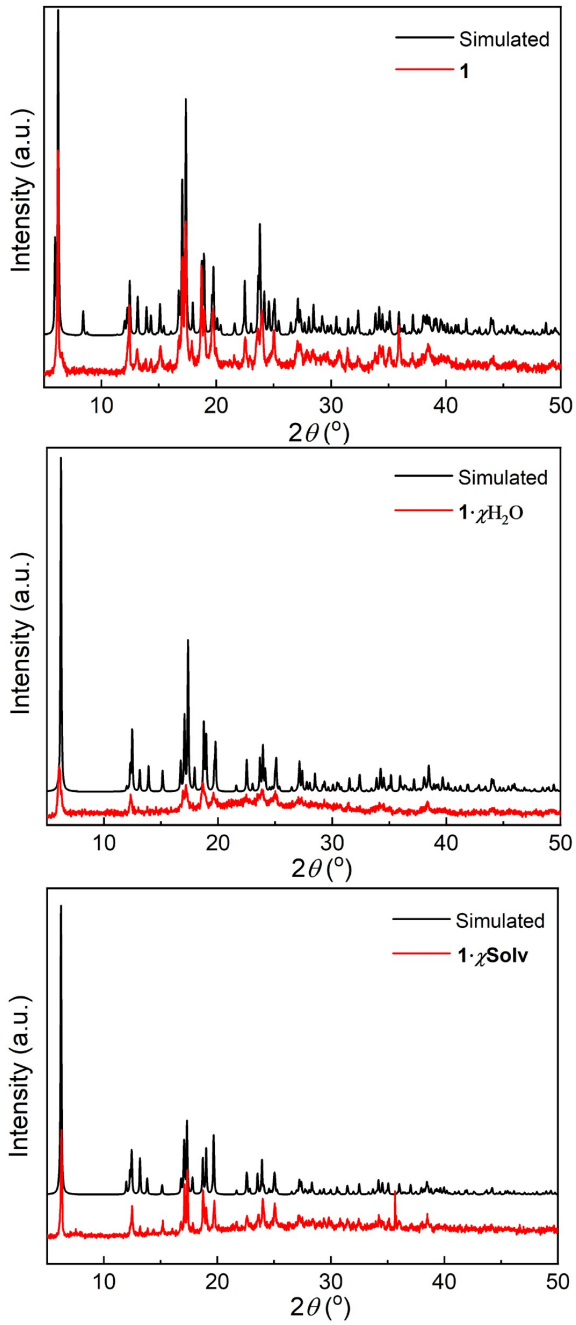

Fig. S5 Comparison of the XRD patterns of **1·*x*H₂O (a)**, **1 (b)**, and **1·*x*Solv (c)** measured from powders and fitted to the single-crystal structure. The high consistency of measurements and simulations confirms the phase purity of samples.

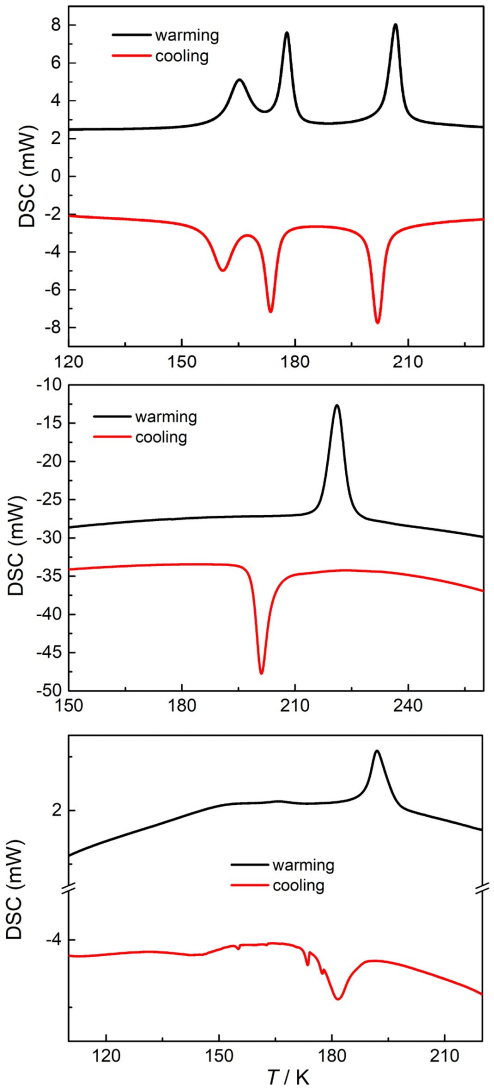

Fig. S6 DSC curves of **1·*x*H$_2$O** (top), **1** (middle), and **1·*x*Solv** (bottom) upon cooling and warming. The exothermic/endothermic peaks in the DSC curves correspond to the spin crossover transitions in the magnetic measurements.

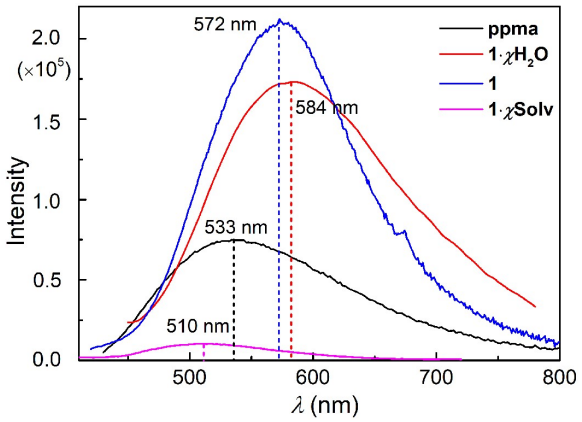

Fig. S7 Solid-state fluorescence spectra of **1·*x*H$_2$O**, **1**, **1·*x*Solv** and **ppma** at room temperature. Excitation: 380 nm.

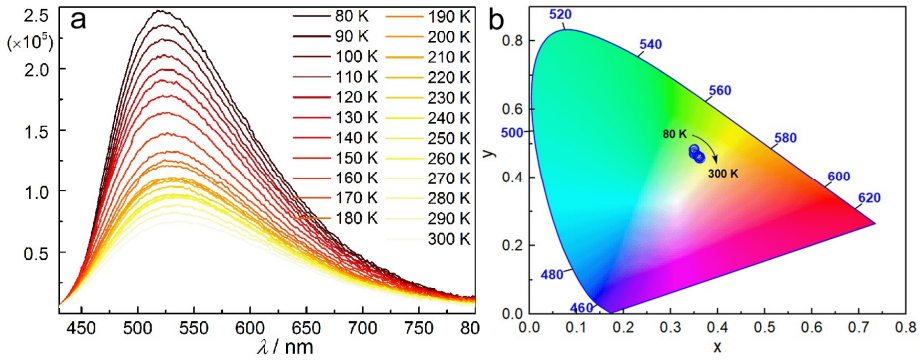

Fig. S8 (a) Temperature-dependent fluorescent spectra and (b) the CIE 1931 (x, y) chromaticity diagram of **ppma** in the solid states (80 K-300 K). Excitation: 380 nm.

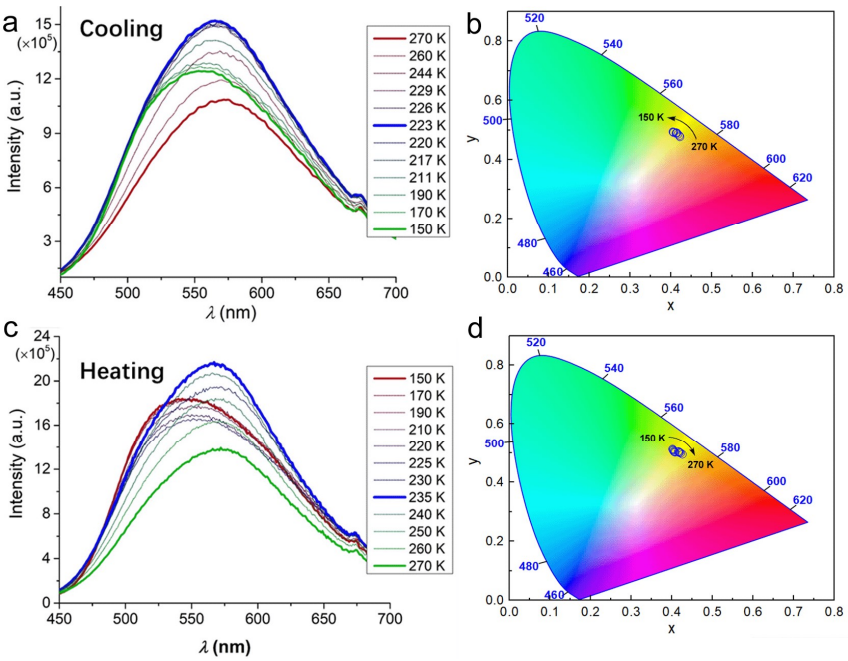

Fig. S9 Temperature-dependent fluorescent spectra (a, c) and the CIE 1931 (x, y) chromaticity diagram (b, d) of **1** in the solid states upon cooling (a, b) and heating (c, d) at λ_{ex} = 380 nm. Notably, the maximum emissions of the sample demonstrate a significant redshift as the temperature increases.

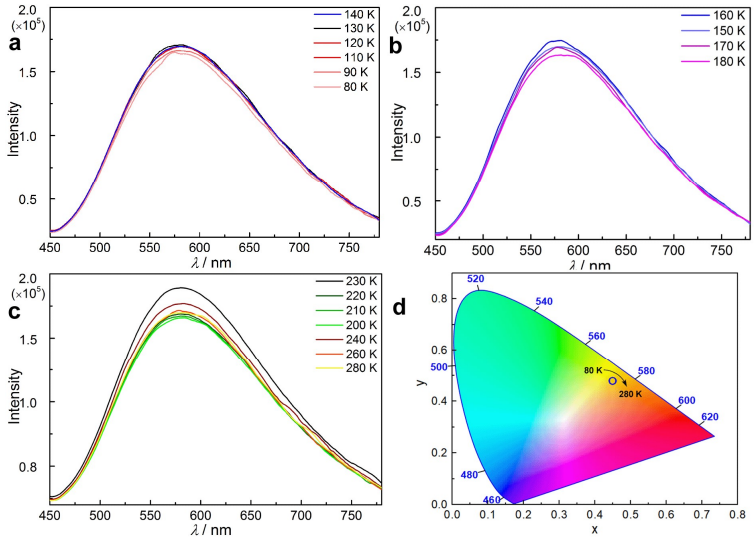

Fig. S10 Temperature-dependent fluorescent spectra of **1·*x*H₂O** in the solid states at different temperature ranges upon heating (a) 80-140 K. (b) 150-180 K. (c) 200-280 K at λ_{ex} = 380 nm. (d) The CIE 1931 (x, y) chromaticity diagram of **1·*x*H₂O** at different temperature ranges upon heating (80-280 K).

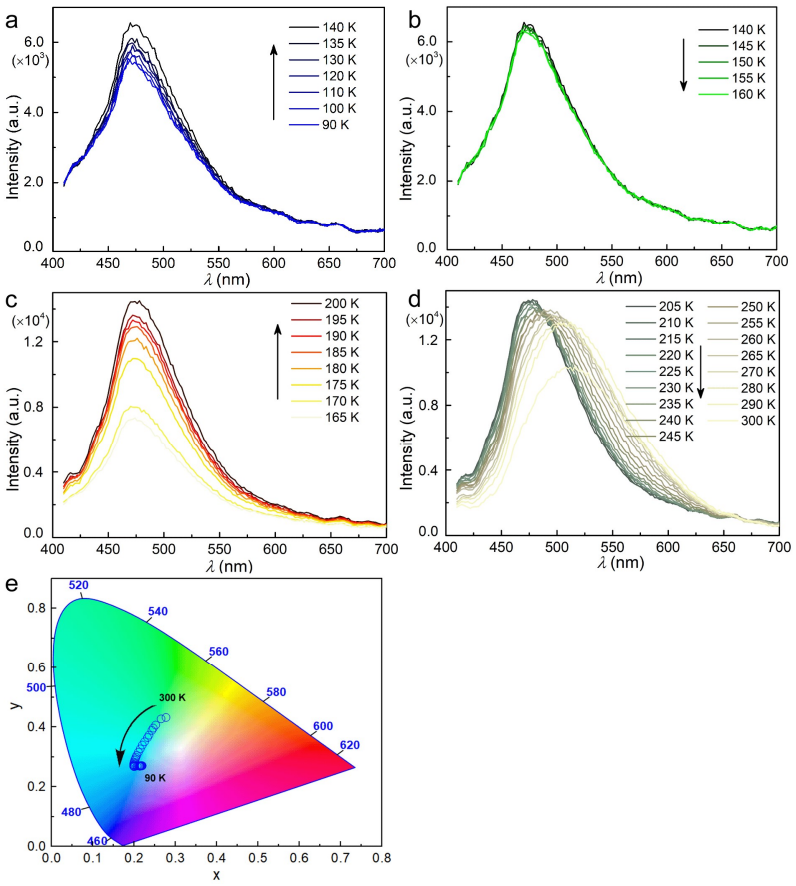

Fig. S11 Temperature-dependent fluorescent spectra of **1**·***x*Solv** in the solid states at different temperature ranges upon cooling (a) 90-140 K. (b) 140-160 K. (c) 165-200 K and (d) 205-300 K at λ_{ex} = 380 nm. Apart from the change of the fluorescent intensity, the maximum emissions also demonstrate a remarkable blueshift upon cooling, particularly in the temperature range of 205-300 K. (e) The CIE 1931 (x, y) chromaticity diagram of **1**·***x*Solv** at different temperature ranges upon cooling (90-300 K).

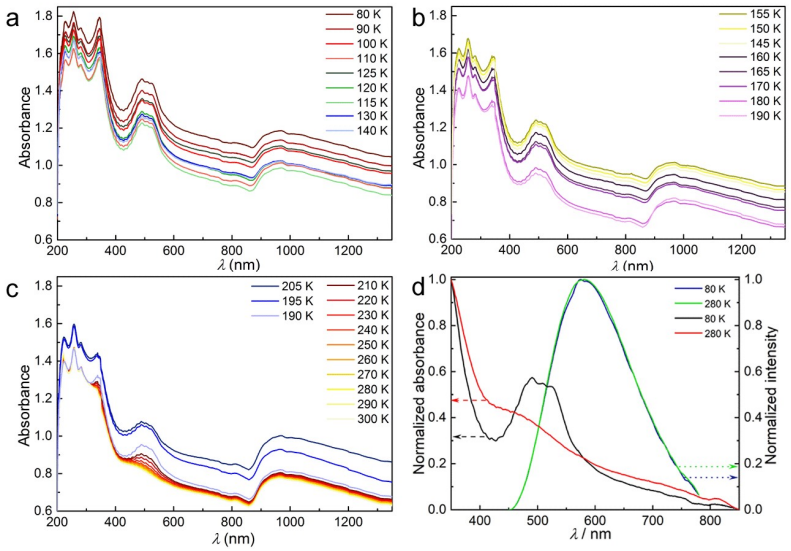

Fig. S12 (a-c) Temperature-dependent UV-Vis spectra of **1**·*x***H₂O** in the range of 80-300 K. (d) Normalized UV-Vis and fluorescence emission spectra of **1**·*x***H₂O** in LS (80 K) and HS states (280 K).

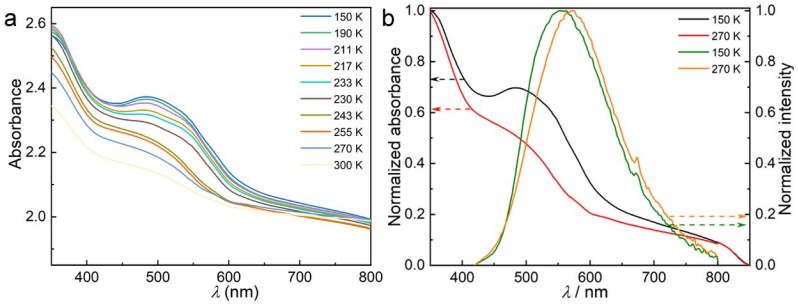

Fig. S13 (a) Temperature-dependent UV-Vis spectra of **1** in the range of 150-270 K. (b) Normalized UV-Vis and fluorescence emission spectra of **1** in LS (150 K) and HS states (270 K).

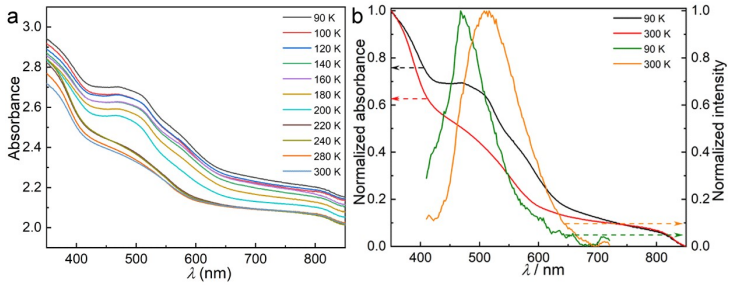

Fig. S14 (a) Temperature-dependent UV-Vis spectra of **1**·*x***Solv** in the range of 90-300 K. (b) Normalized UV and fluorescence emission spectra of **1**·*x***Solv** in LS (90 K) and HS states (300 K).

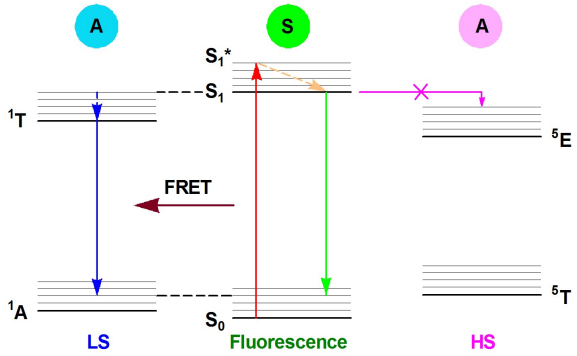

Fig. S15 Schematic illustration of the FRET mechanism between the centres sensitizer (S stands for **ppma**) and acceptor (A stands for **Fe**).

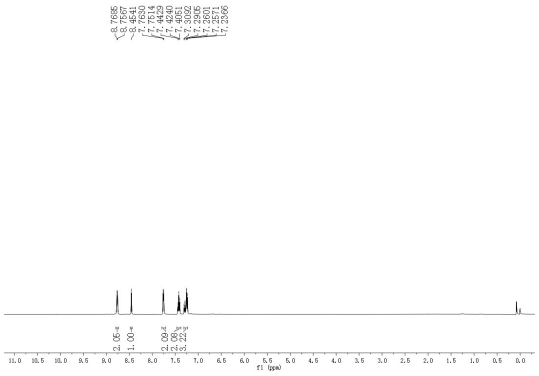

Fig. S16 ^{1}H NMR spectra of **ppma** in $CDCl_3$.

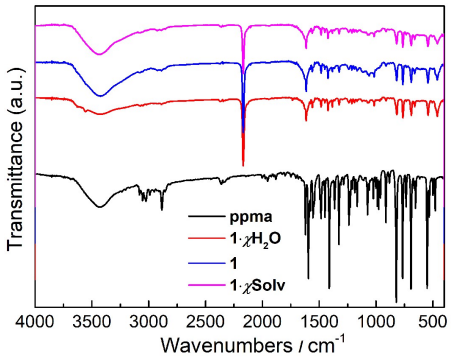

Fig. S17 FT-IR spectra of **ppma**, **1**·*x*$\mathbf{H_2O}$, **1**, and **1**·*x***Solv**.